Supporting Information for 'Radar characterization of ice crystal orientation fabric and anisotropic rheology within an Antarctic ice stream'

T. M. Jordan [1,2,3], C. Martin [4], A. M. Brisbourne [4], D. M. Schroeder [2,5], and

A. M. Smith [4]

[1]School of Geographical Sciences, University of Bristol, Bristol, UK.

[2]Department of Geophysics, Stanford University, Stanford, USA.

[3]Plymouth Marine Laboratory, Plymouth, UK.

[4]British Antarctic Survey, Cambridge, UK.

[5]Department of Electrical Engineering, Stanford University, Stanford, USA.

Contents of this file

1. Supporting information for polarimetric data analysis methodology.
2. Polarimetric coherence analysis at all measurement sites.
3. Polarimetric coherence analysis for the full ice column.
4. Sensitivity of fabric estimates to different coherence window sizes.

1. Supporting information for polarimetric data analysis methodology.

Figure S1 shows a flow-diagram illustrating the key steps of the polarimetric coherence method. To take into account measurement uncertainty the data-fits are performed over a set of 50 ensemble members incorporating azimuthal error on the antenna alignment and coherence phase uncertainty. Steps 2,3 and 5 run over each ensemble member.

In Step 2 we account for alignment uncertainty assuming σ_θ=$\pm$ 5° which is modeled as a Gaussian random variable for each measured HV mode combination. We account for coherence uncertainty in Step 3 by then perturbing each ϕ_{hhvv} pixel with the phase error, $\sigma_{\phi_{hhvv}}$ (see equation (3) in the main article), again modeled as a Gaussian random variable. The phase derivative, $\frac{\phi_{hhvv}}{dz}$, which is used directly in the fabric estimation, is then computed within Step 3 for each ensemble member with these two sources of uncertainty incorporated.

The data-fits in Step 5 are carried for each ensemble member using the azimuthal symmetry constraint for $\frac{\phi_{hhvv}}{dz}$ about $\theta = \theta_G$. This is illustrated visually in Figure 4 in the main article, using synthetic data and the backscatter model, Step 4. To computationally implement the constraint, and solve for $\theta_G(z)$ at each ice depth, we minimize a cost function in each range bin of the form

$$\theta_G = \arg\min_{\theta_n} \left\{ \sum_{\theta_n=0^\circ}^{\theta_n=180^\circ} \sum_{\theta_m=0^\circ}^{\theta_m=180^\circ} w_m \sqrt{\left(\frac{d\phi_{hhvv}}{dz}(\theta_n+\theta_m) - \frac{d\phi_{hhvv}}{dz}(\theta_n-\theta_m) \right)^2} \right\}, \quad (1)$$

where w_m is a normalization weight and the indices n and m run over all of the azimuthal pixels (181 assuming an angular resolution of 1°). In the ideal case, when there is perfect reflection symmetry about θ_G, each $\left(\frac{d\phi_{hhvv}}{dz}(\theta_n+\theta_m) - \frac{d\phi_{hhvv}}{dz}(\theta_n-\theta_m)\right)$ term in the summation over θ_m is zero, and the minimization results in $\theta_n = \theta_G$ (or $\theta_n = \theta_G \pm 90^\circ$) at a

given ice depth. Once the profile $\theta_G(z)$ is obtained, $G(z)$ is obtained using equation (4) in the main article.

Steps 2-5 repeat over all ensemble members, and ensemble means and standard deviations evaluated at each ice depth give the mean and propagated uncertainty for $\theta_G(z)$ and $G(z)$.

2. Polarimetric coherence analysis at all measurement sites

Figures S2 and S3 show polarimetric coherence analysis for sites along Transect A that were not included in the main article. As in the main article, we assume a vertical girdle description of the fabric (corresponding horizontal pole parameters can be obtained from $\theta_P = \theta_G$ and $P = \frac{G}{2}$). The series of plots illustrates the relative counter-clockwise rotation of $\theta_G(z)$ in shallow ice as the measurements become closer to the shear margin. The increase in G in shallower ice toward the shear margin is also evident from the faster phase cycles.

Figures S4 and S5 show polarimetric coherence analysis for additional sites along Transect B. Sites B3-B5, Figure S5, are all qualitatively similar to site B2 shown in the main article. Site B7 has a negligible phase gradient in shallower ice, Figure S5b. This is likely to correspond to a near-random fabric (as the vertical fabric eigenvalue is likely to be relatively low in shallower ice). Sites B8 and B9, Figure S5b and c, show a qualitatively similar azimuthal rotation for $\theta_G(z)$ within the ice column ($\approx 90^\circ$ at z $\approx$ 100 m) to site B10 in the main article.

3. Polarimetric coherence analysis for the full ice column

Figure S6 shows polarimetric coherence analysis for the full ice column at sites A1 and A6. In general, the coherence magnitude is not sufficiently high to make accurate fabric estimates throughout the ice column (based on the filtering step which requires $|c_{hhvv}(\theta_G, z)| > 0.5$). In deeper ice ($z > 1400$ m), however, there is a unit of high coherence magnitude where fabric estimates can be made. In this unit the vertical phase gradient is negligible, which results in locally fluctuating estimates for θ_G and negligible estimates for G. The estimates in this unit therefore support the existence of a tendency toward a vertically-orientated single maximum fabric (as the vertical fabric eigenvalue is likely to be high in deeper ice).

4. Sensitivity of fabric estimates to different coherence window sizes

Figure S7 shows the sensitivity of fabric estimates along Transect A for three different window sizes, W. An example of the coherence analysis for one of the sites (A6) is shown in Figure S8. The θ_G estimates are highly robust to the window size, and fall within the estimated uncertainty bounds, Figure S7a. The G estimates have a systematic decrease with window size, Figure S7b, although all window sizes capture the important trend of strengthening toward the shear-margin (sites A5-A9). The choice of W=40 m in the main article is thought to represent a good trade-off between desired vertical resolution and including enough range-cells to produce a robust coherence estimate.

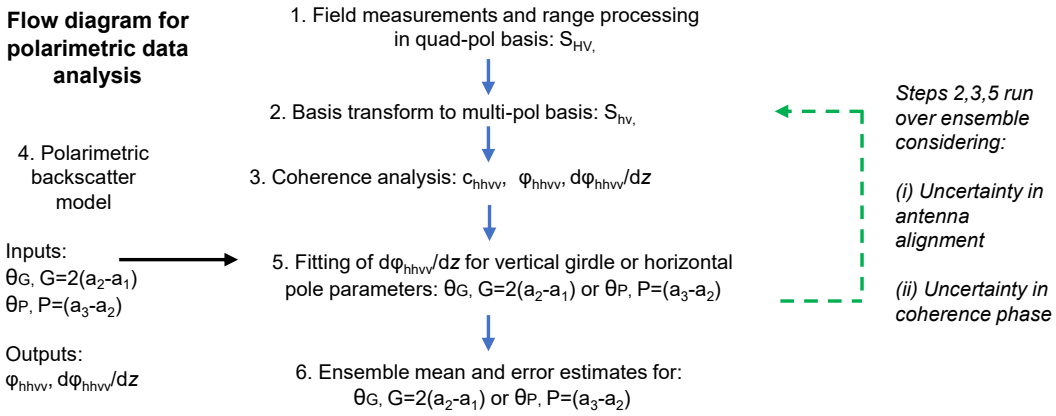

Figure S1. Flow diagram for polarimetric data analysis.

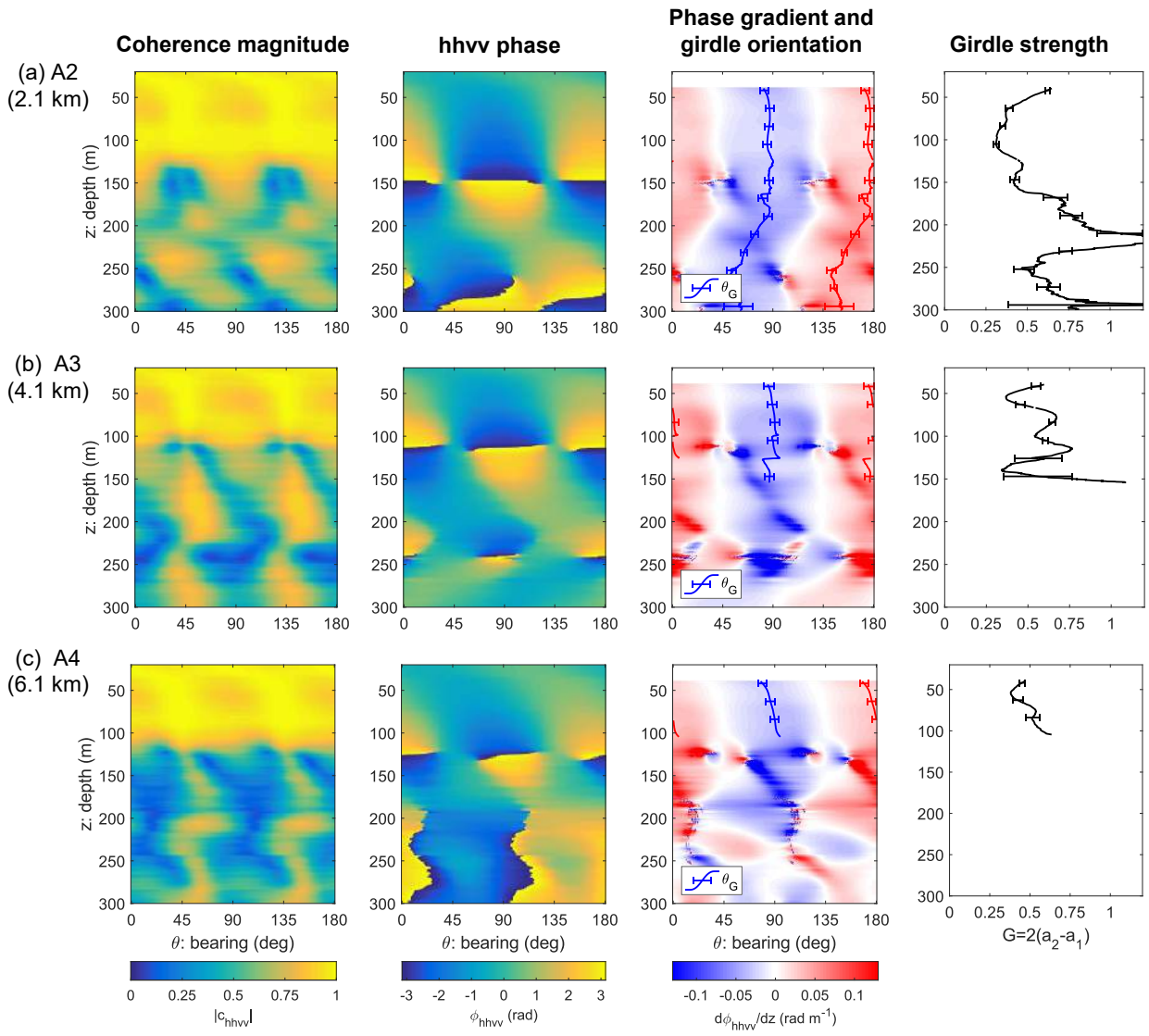

Figure S2. Polarimetric coherence analysis at sites: (a) A2, (b) A3, (c) A4. The depth-profiles for the girdle fabric estimates, $\theta_G(z)$ and $G(z)$ are shown in the center right and far right columns. A filtering step is applied such that fabric estimates require $|c_{hhvv}(\theta_G, z)| > 0.5$.

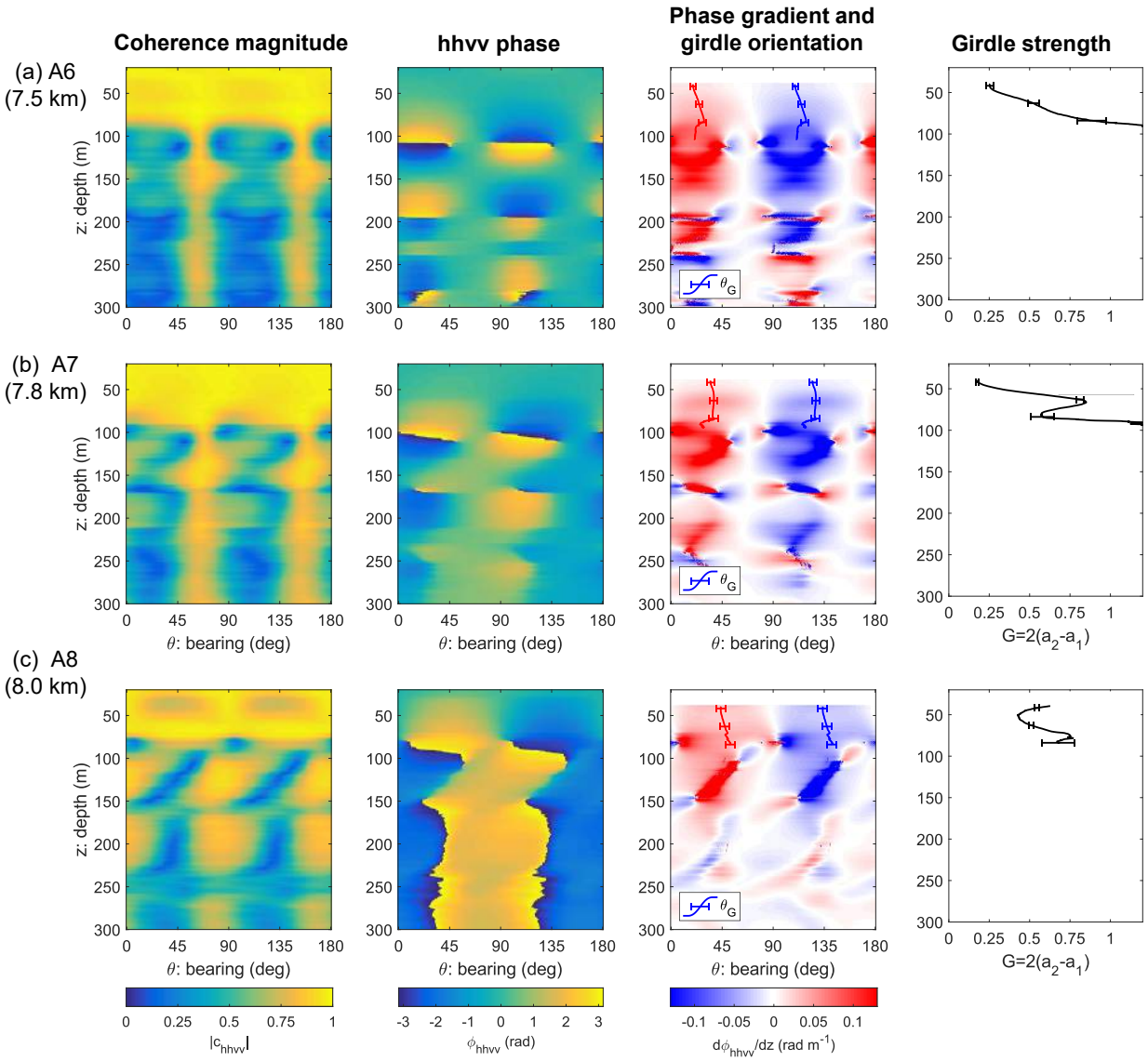

Figure S3. Polarimetric coherence analysis at sites: (a) A6, (b) A7, (c) A8.

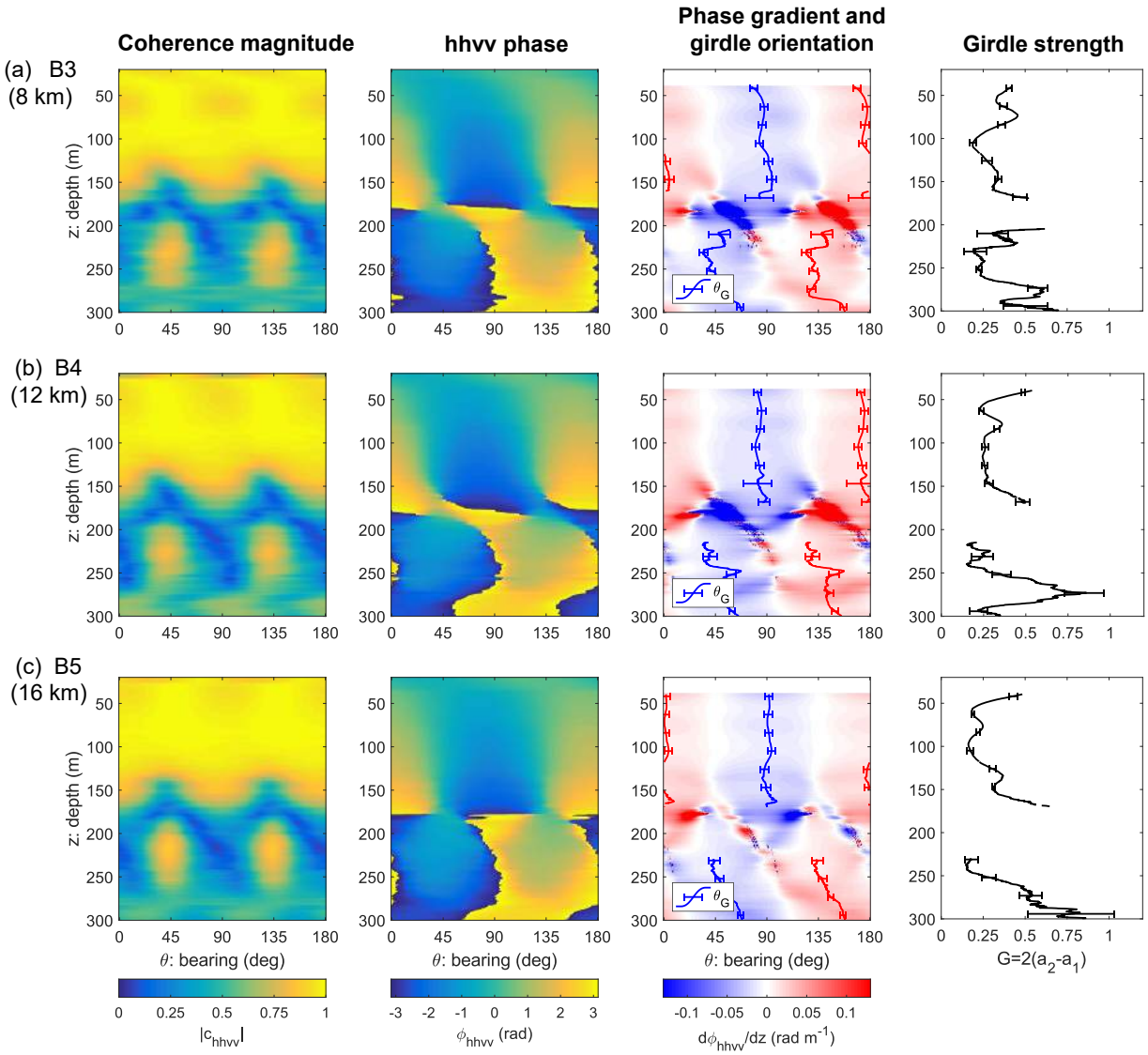

Figure S4. Polarimetric coherence analysis at sites: (a) B3, (b) B4, (c) B5.

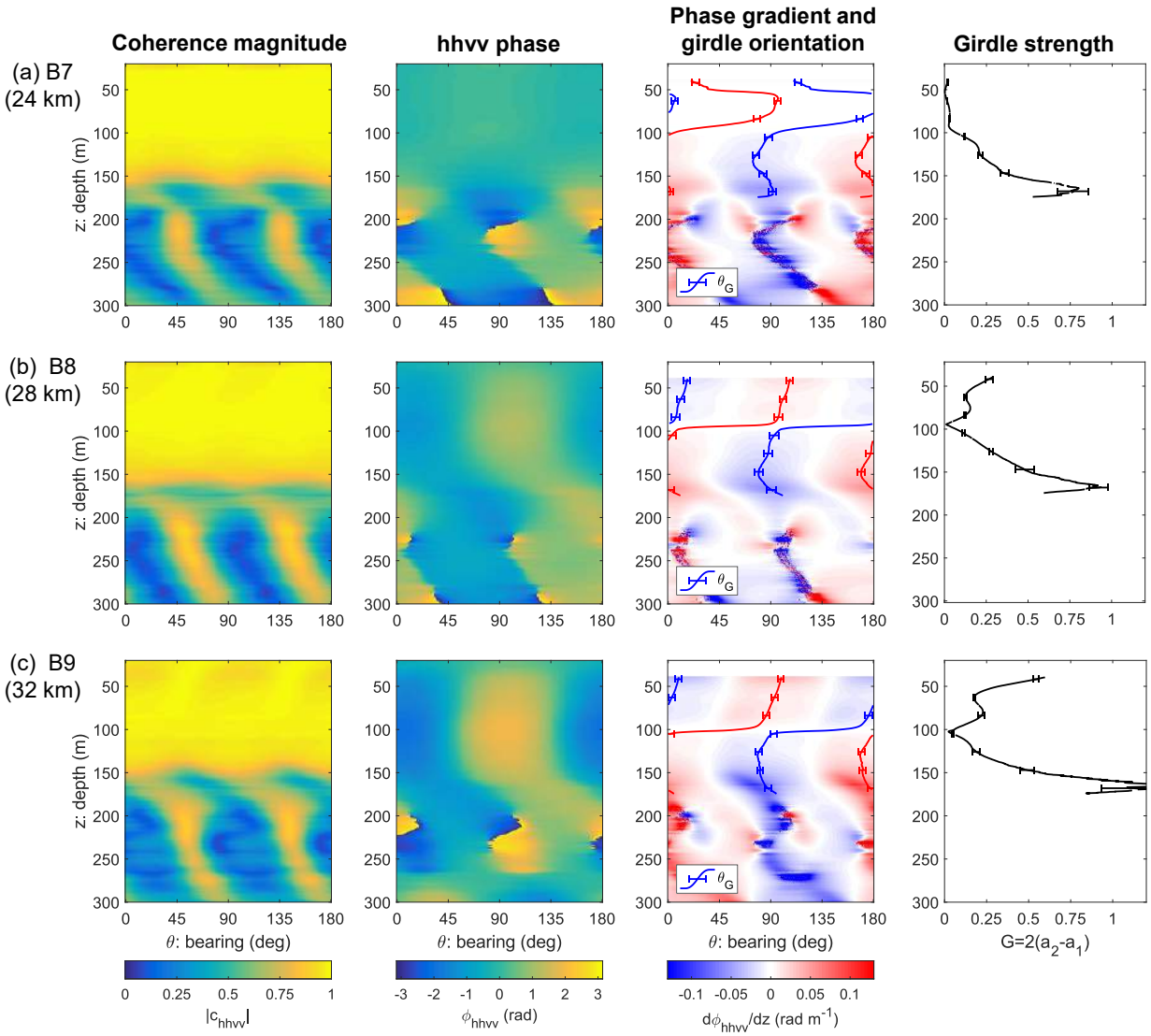

Figure S5. Polarimetric coherence analysis at sites: (a) B7, (b) B8, (c) B9.

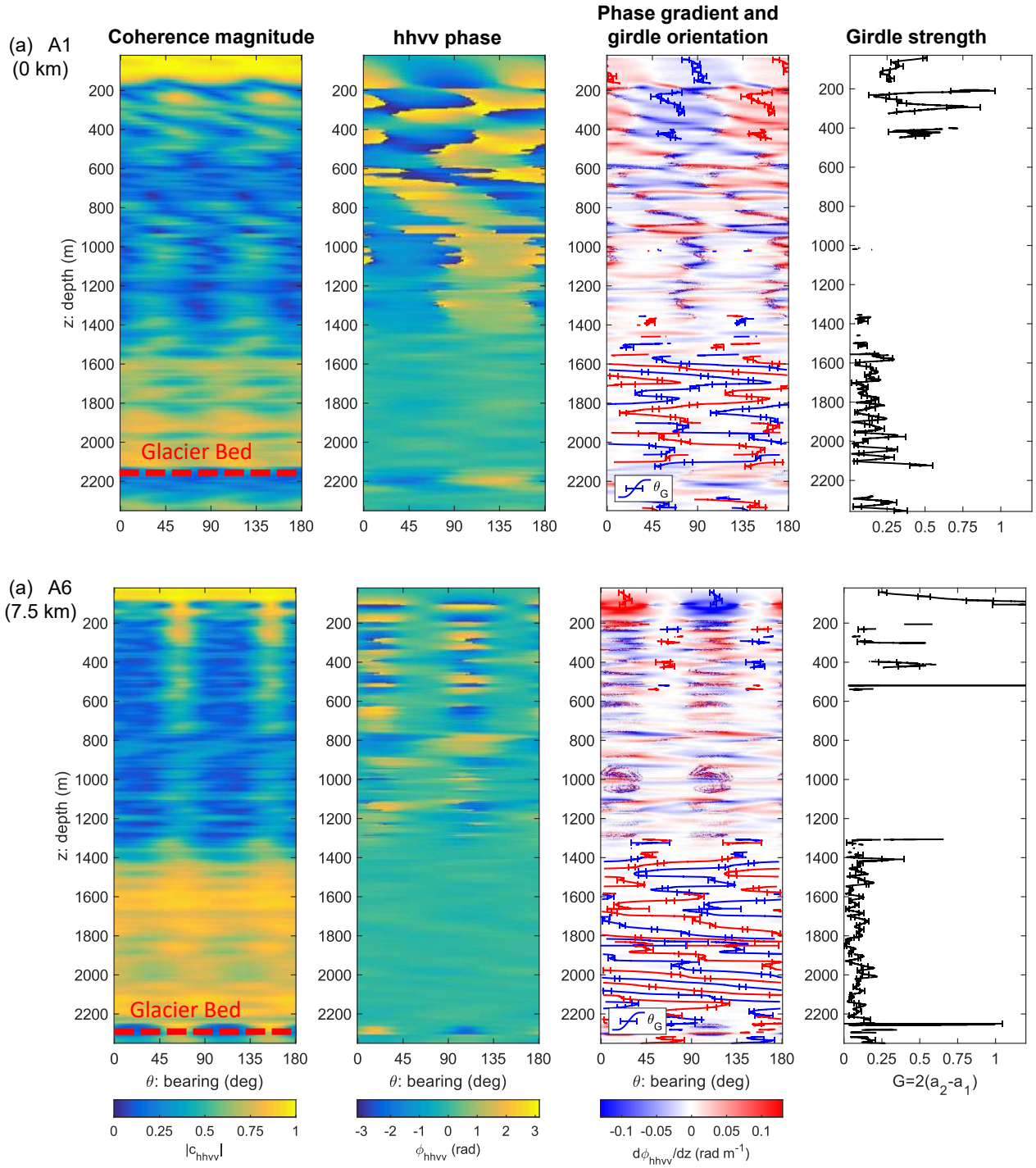

Figure S6. Full ice column polarimetric coherence analysis at sites: (a) A1, (b) A6.

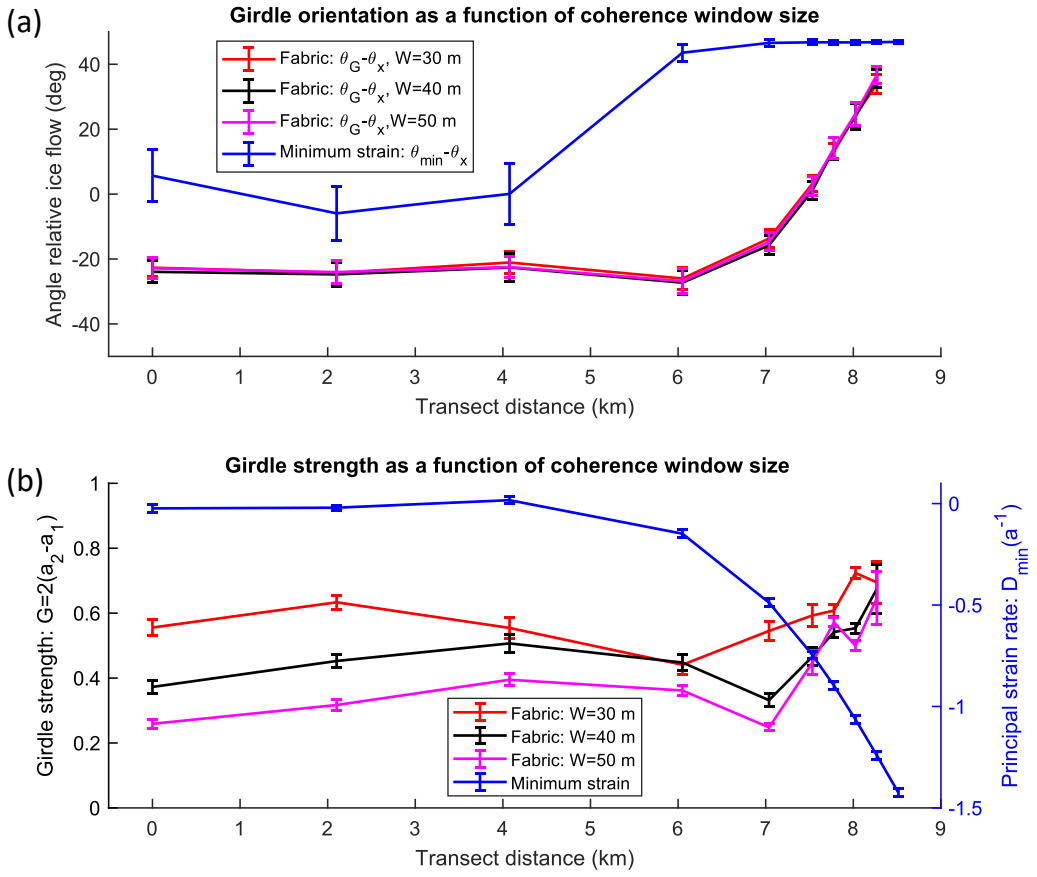

Figure S7. Sensitivity of fabric estimates for three different different window sizes, W (Transect A). (a) Girdle orientation in relation to ice flow, $(\theta_G - \theta_x)$. (b) Girdle Strength, G.

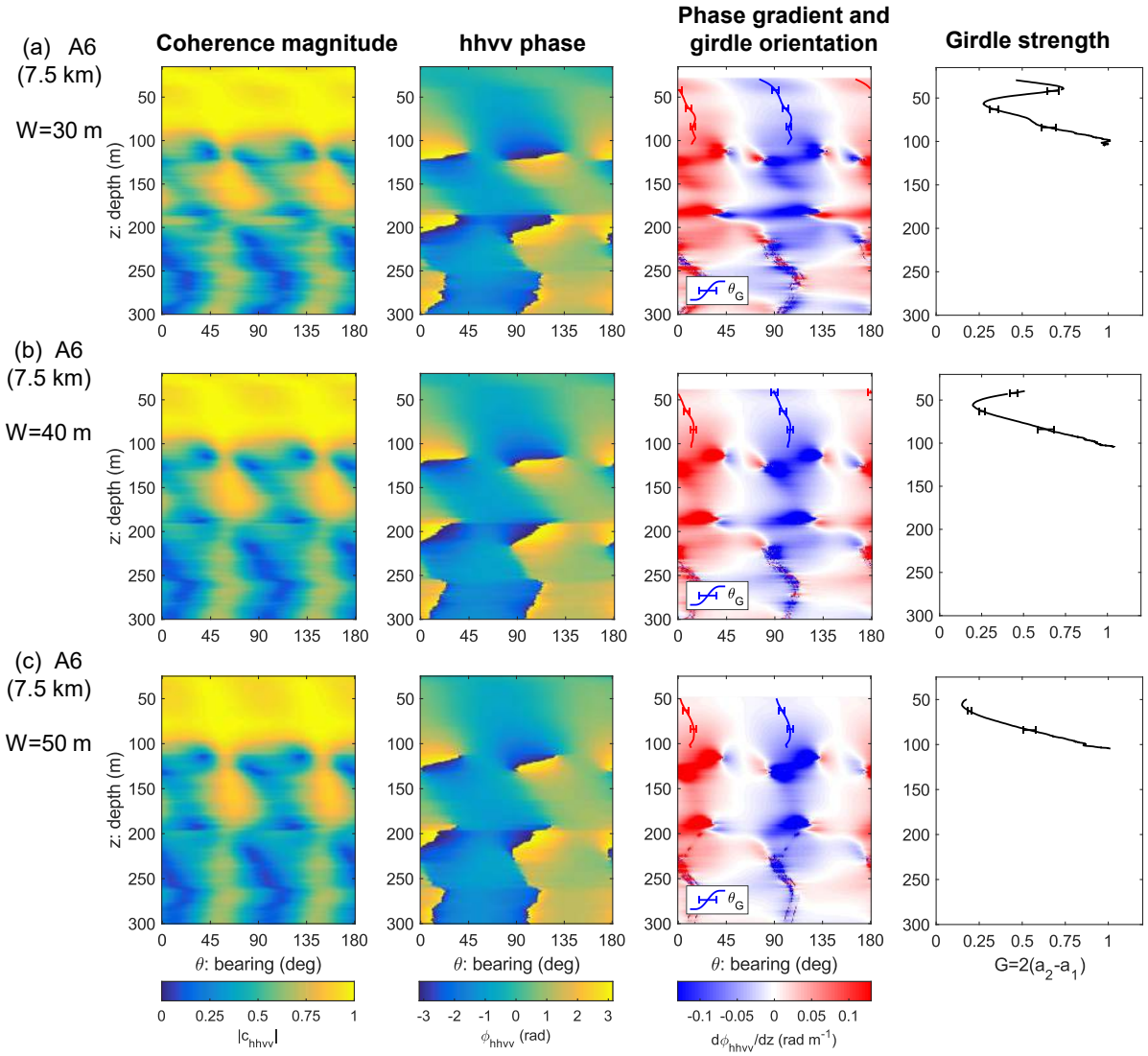

Figure S8. Polarimetric coherence analysis at site A6 for three different window sizes, W. (a) W=30 m. (b) W=40 m. (c) W=50 m.